AMERICAN ACADEMY OF OPHTHALMOLOGY®

Deep Learning-Based Prediction of Individual Geographic Atrophy Progression from a Single Baseline OCT

Julia Mai, MD, Dmitrii Lachinov, MSc, Gregor S. Reiter, PhD, Sophie Riedl, PhD, Christoph Grechenig, MD, Hrvoje Bogunovic, PhD, Ursula Schmidt-Erfurth, MD

Objective: To identify the individual progression of geographic atrophy (GA) lesions from baseline OCT images of patients in routine clinical care.

Design: Clinical evaluation of a deep learning-based algorithm.

Subjects: One hundred eighty-four eyes of 100 consecutively enrolled patients.

Methods: OCT and fundus autofluorescence (FAF) images (both Spectralis, Heidelberg Engineering) of patients with GA secondary to age-related macular degeneration in routine clinical care were used for model validation. Fundus autofluorescence images were annotated manually by delineating the GA area by certified readers of the Vienna Reading Center. The annotated FAF images were anatomically registered in an automated manner to the corresponding OCT scans, resulting in 2-dimensional en face OCT annotations, which were taken as a reference for the model performance. A deep learning-based method for modeling the GA lesion growth over time from a single baseline OCT was evaluated. In addition, the ability of the algorithm to identify fast progressors for the top 10%, 15%, and 20% of GA growth rates was analyzed.

Main Outcome Measures: Dice similarity coefficient (DSC) and mean absolute error (MAE) between manual and predicted GA growth.

Results: The deep learning-based tool was able to reliably identify disease activity in GA using a standard OCT image taken at a single baseline time point. The mean DSC for the total GA region increased for the first 2 years of prediction (0.80−0.82). With increasing time intervals beyond 3 years, the DSC decreased slightly to a mean of 0.70. The MAE was low over the first year and with advancing time slowly increased, with mean values ranging from 0.25 mm to 0.69 mm for the total GA region prediction. The model achieved an area under the curve of 0.81, 0.79, and 0.77 for the identification of the top 10%, 15%, and 20% growth rates, respectively.

Conclusions: The proposed algorithm is capable of fully automated GA lesion growth prediction from a single baseline OCT in a time-continuous fashion in the form of en face maps. The results are a promising step toward clinical decision support tools for therapeutic dosing and guidance of patient management because the first treatment for GA has recently become available.

Financial Disclosure(s): Proprietary or commercial disclosure may be found in the Footnotes and Disclosures at the end of this article. *Ophthalmology Science 2024;4:100466*

Supplemental material available at www.ophthalmologyscience.org.

Geographic atrophy (GA) represents a chronic degenerative disease, which leads to progressive and irreversible loss of retinal tissue and function. Geographic atrophy is the advanced stage of nonneovascular age-related macular degeneration (AMD), which is a leading cause of blindness in developed countries.[1] The majority of all AMD patients are affected by the nonneovascular AMD type as this is the natural course of the disease. To date, $\geq$ 1 million patients in the United States and 8 million patients worldwide are affected by GA secondary to AMD, with an even higher estimated number of unknown cases.[2–5] Current treatment concepts for GA secondary to AMD aim to slow disease progression.[6,7] Different imaging modalities can be used to monitor GA development and progression, including fundus autofluorescence (FAF) and OCT.[8] On FAF, GA appears as sharply demarcated hypoautofluorescent regions. However, FAF imaging in GA is limited to the 2-dimensional retinal pigment epithelium (RPE) layer. Moreover, the evaluation of foveal involvement is difficult, as the macular pigment blocks blue light in the central macula.[6] OCT offers substantial advantages and additional information in the assessment of GA lesions compared with FAF. Particularly through the comprehensive visualization of retinal components like

https://doi.org/10.1016/j.xops.2024.100466
ISSN 2666-9145/24

the photoreceptor layer, OCT allows for a more detailed insight into the pathomorphological changes.[9] Moreover, high-resolution OCT is very sensitive for the identification of early atrophy and therefore provides a better understanding of GA precursors and progression.[10]

In clinical trials, the change in FAF-derived GA growth rate has been used as the primary end point for evaluating any potential therapeutic efficacy.[11] A recent meta-analysis revealed a pooled mean GA growth rate between 1.66 mm^2/year and 0.33 mm/year.[12] However, it has been shown abundantly that the progression rates in GA are highly variable among patients ranging from 0.53 to 2.6 mm^2 per year.[13] Like in neovascular AMD, treatment requirements may be correlated with disease activity, i.e., the speed of progression on an individual patient level. Being able to predict the progression rate on an individual basis as well as identifying fast and slow progressors would allow for optimal patient counseling and personalized treatment, introducing standardized therapeutic guidelines into the management of millions of individuals. Moreover, the design and analysis of treatment studies would strongly benefit from the identification of patients with different levels of disease activity and progression profiles.

The aim of this study was to clinically validate a deep learning-based algorithm to predict the individual GA progression rate from a single baseline OCT volume over the time span of 3 years using patient data from routine clinical care. Additionally, the ability of the algorithm to identify fast progressors, i.e., patients with the fastest-growing lesions, was evaluated.

Methods

Data Set and Study Population

Spectral-domain (SD)-OCT scans and FAF images (both Spectralis, Heidelberg Engineering) of patients with GA secondary to AMD from the outpatient clinic at the Medical University of Vienna were analyzed and used for model development and validation.

The study population consisted of 184 eyes of 100 patients who were consecutively enrolled from routine clinical care. Patients were $\geq$ 50 years of age and had a diagnosis of GA on FAF, secondary to nonneovascular AMD, assessed by 2 experienced graders. A detailed description has been previously published.[14] Patients were excluded if there was a history of other ocular diseases that would confound retinal assessment. Patients were followed up every 3 months for $\geq$ 12 months, and FAF and SD-OCT scans were performed at every visit. Fundus autofluorescence images were excluded in case of insufficient image quality preventing accurate measurement of lesion size.

The presented study was approved by the ethics committee of the Medical University of Vienna (EK Nr: 1246/2016). All research was performed in compliance with the tenets of the Declaration of Helsinki and Good Clinical Practice. Written informed consent was given by all patients for future medical research and analyses.

Image Analysis and FAF to OCT Reference Annotations

Fundus autofluorescence images were annotated manually by delineating the GA area, defined as well-demarcated areas with a significantly decreased or extinguished degree of autofluorescence by certified readers of the Vienna Reading Center, using a validated image analysis software (OCTAVO, Vienna Reading Center). Moreover, all FAF images were graded at baseline for the perilesional FAF patterns, the presence of a multilobular lesion configuration, and the presence or absence of subretinal drusenoid deposits as previously described.[14] To obtain matched OCT gradings, annotated FAF images were anatomically registered in an automated manner to the corresponding near-infrared reflectance images, which were aligned with the acquired OCT scans by the imaging device, resulting in 2-dimensional en face OCT annotations. A deep learning-based spatial registration method was employed,[15] and the registration process corrected the difference in magnification between the FAF image and the OCT scan. The resulting OCT annotations were taken as ground truth for training and as a reference for the model performance. OCT offers more detailed information on the pathologic changes in different retinal layers in GA compared with FAF. By taking the entire 3-dimensional volume into account, the algorithm benefits from rich spatial information instead of just looking at an en face reflectance map. We believe that this is a more precise approach to segment GA by accurately segmenting the RPE loss on every B-scan and subsequently creating an en face map.

Model Development

In this study, a newly developed method for modeling the progression of GA lesion growth over time from a single baseline SD-OCT scan was used. The technical framework of the algorithm has been published in detail.[16] In summary, the method takes a single OCT volume as an input and extracts feature encodings of each A-scan using PSC-UNet with projective skip-connections that compress the encoded features in the A-scan dimension.[17] These feature encodings represent the current state of the GA lesion at a given A-scan. The time derivative at the provided feature encoding is approximated using another convolutional neural network. With known feature encodings of the baseline image corresponding to the initial conditions and the learned time-derivative function of the feature encodings, the initial value problem is defined. To solve it, the Runge–Kutta fourth order numerical method is used to obtain the feature encodings at the future time t. In this work, we opt for a method that can handle a large family of ordinary differential equations (ODEs) produced by NeuralODE, sacrificing some accuracy. In general, employing implicit methods in the context of Neural ODEs greatly increases computational requirements and impacts the stability due to potential convergence problems of Newton's iteration at each time step caused by highly nonlinear NeuralODE. From the family of explicit methods, we found fourth order-Runge-Kutta to be the best suitable for the task, as the Euler method often struggles even with the simplest ODEs, second or third order Runge–Kutta methods bring no additional benefits, and fifth to fourth order adaptive step methods often produce large computational burden, especially during the training. Once the encoded features are obtained for each individual A-scan, they are further transformed into the probability of GA at the given A-scan using a linear layer. The learning of the time derivative approximation is enabled by the algorithm described by Chen et al.[18] The model is then able to predict the location of the GA lesion growth at a future time point in the form of an en face segmentation map and enables a continuous-time predicted GA localization. The block diagram of the model can be found in Figure S1 (available at www.ophthalmologyscience.org).

Training and Validation

For training and validation, we employed a fivefold cross-validation setup. The clinical data set was split into 5 groups at

the patient level with stratification by the baseline lesion size. Five instances of the segmentation model were trained. For each instance, 1 group was selected as the validation set and the remaining 4 groups as the training set. After the training, each model processed the corresponding validation set. The results from the 5 validation sets were pooled together and the segmentation performance metrics described below were computed. For training, we sampled 2 visits of a single patient with a time difference of 6 to 12 months, thus, a single patient could produce multiple paired visits, effectively augmenting the training data set. The network was asked to process the first visit and reconstruct the GA segmentation of both the first and second visits. For validation, the whole patient history was utilized. We processed the baseline OCT with the trained network and compared the network outputs with the observed patient history.

Statistical Analysis

The performance of the algorithm was evaluated by calculating the mean ± standard deviation of the dice similarity coefficient (DSC), representing the overlap between the predicted topographic GA region and the manual ground truth for the total GA region and for the GA growth region. The GA growth region was defined as the difference between the GA region at the follow-up visit and the baseline visit. To adjust for baseline lesion size, the GA growth rate was calculated using the previously established square root transformation by calculating the difference between the square root of the baseline and the square root of the respective follow-up visit.[19] Additionally, the mean absolute error (MAE) ± standard deviation for the square root transformed total GA region and GA growth region was computed. The correlation between the manual and predicted growth rates was reported using Pearson correlation coefficient r and the coefficient of determination R^2. The ability of the algorithm to identify fast progressors for different cut-off values (the top 10%, 15%, and 20%) of GA lesion growth rates was evaluated using the area under the curve with 95% confidence interval. All statistical analyses were done using Python, sklearn, and scipy.

Results

Data Set and Baseline Characteristics

For training and validation, 967 OCT volumes (at all time points) from 184 study eyes of 100 patients were used from routine clinical care at the outpatient clinic. The mean age was 76.2 ± 7.6 years and 64% were female. The mean square root transformed baseline GA area was 2.4 mm (95% confidence interval 2.28−2.58 mm) and the mean square root transformed GA growth rate was 0.32 mm (95% confidence interval 0.29−0.35 mm) per year. The baseline characteristics of the study population are summarized in Table 1.

Table 1. Baseline Characteristics of the Study Population

Data Type	Data
Number of patients	100
Number of eyes	184
Baseline age (yrs), mean (SD)	76.2 (7.6)
Female gender, n (% patients)	64 (64)
Follow-up period (mos), mean (IQR)	32 (24-36)
Baseline GA area (mm), mean (95% CI)	2.43 (2.28−2.58)
GA growth rate (mm/yr), mean (95% CI)	0.32 (0.29−0.35)
Baseline FAF patterns, n (% eyes)	
Focal	34 (18.5)
Banded	39 (21.2)
Diffuse	87 (47.3)
Diffuse-trickling	11 (6.0)
Patchy	1 (0.5)
None	11 (6.0)
Ungradable	1 (0.5)
Baseline multilobular configuration, n (% eyes)	
Yes	44 (23.9)
No	117 (63.6)
Ungradable	23 (12.5)
Baseline SDD, n (% eyes)	
Yes	112 (60.9)
No	62 (33.7)
Ungradable	10 (5.4)

Baseline GA area and GA growth rate are presented as square root transformed values.
CI = confidence interval; FAF = fundus autofluorescence; GA = geographic atrophy; IQR = interquartile range; SD = standard deviation; SDD = subretinal drusenoid deposits.

Geographic Prediction Patterns

Figure 1 visualizes the qualitative results of the GA progression prediction in the format of en face maps over time and their comparison to the manual ground truth annotations. An example of a unifocal and a multifocal GA lesion is illustrated. The prediction pattern is overall reliable and correctly identifies the major lesion component. Precision is highest over the first year, deviations are discrete over as long as 2 years and increase when the follow-up is prolonged to 3 years. At the farthest point in time, lesion growth toward the center is more likely to be affected by false positive prediction, whereas the prediction of peripheral multifocal satellites becomes compromised by false negative prediction. The respective videos are included in the Supplemental Material to illustrate the output of the model as a time-lapse through the GA progression prediction up to 3 years for 1 unifocal lesion (Video 1, available at www.ophthalmologyscience.org) and 1 multifocal lesion (Video 2, available at www.ophthalmologyscience.org).

Precision of Prediction over Time

The performance of predicting the total current and future GA region in terms of DSC is presented in Figure 2A, whereas the performance of predicting the GA growth region over different time intervals is shown in Figure 2B. In addition, Figure 2C, D demonstrate the distribution of square root MAE for the predicted total GA region and the GA growth region, respectively. All metrics are shown for the time intervals between baseline acquisition and the advancing future time points for GA progression prediction. The values for the mean DSC as well as MAE, both for the total GA region and GA growth region, are summarized in Table 2.

The mean DSC for the total GA region at baseline was 0.80 and increased slightly for the first 2 years of prediction with a mean DSC of 0.82 at years 1 and 2. With increasing time intervals beyond 3 years, the DSC decreased slightly to a mean DSC of 0.70. The mean DSC of the GA growth

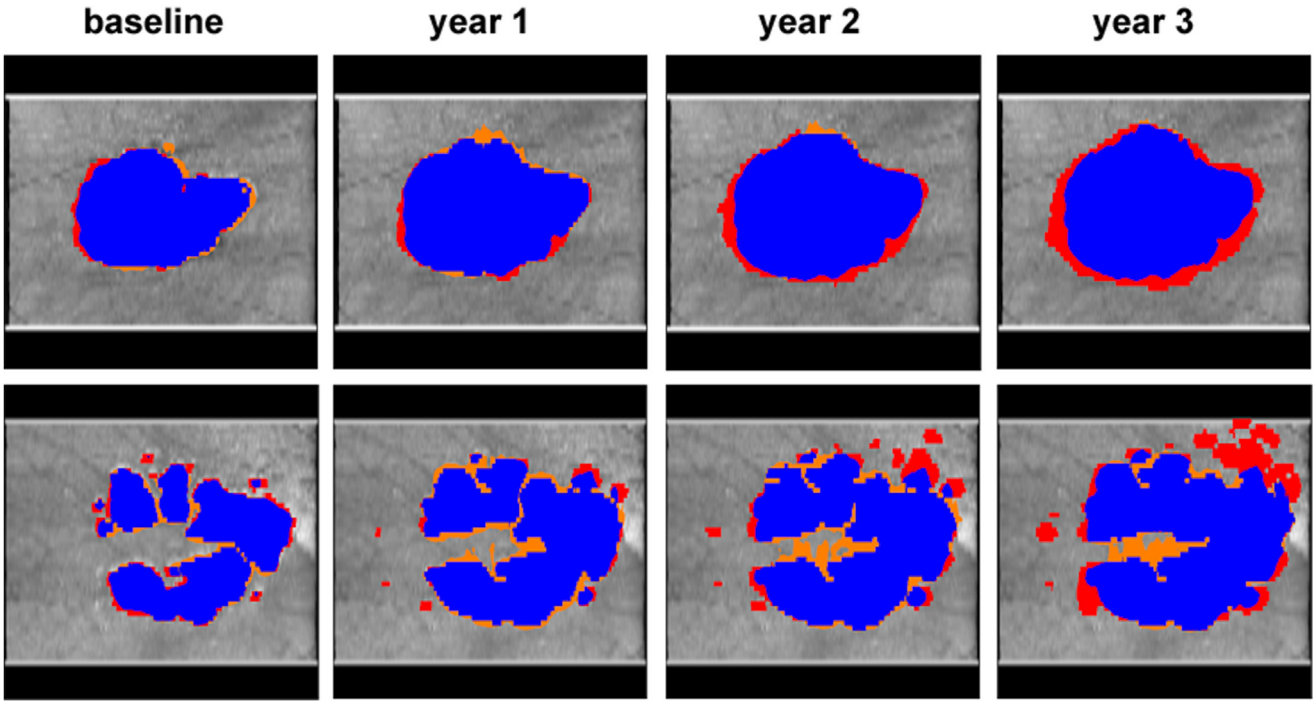

Figure 1. Qualitative examples of predicted geographic atrophy growth for a unifocal lesion (upper row) and multifocal lesion (lower row) over time. blue = true positive prediction; orange = false positive prediction; red = false negative prediction compared with the manual ground truth.

region was 0.25 for the first year of prediction and increased over time to a mean DSC of 0.38 for years 2 and 3. With increasing GA growth over time and therefore larger GA lesion size and accumulating changes in individual disease biology beyond the RPE layer, the DSC is expected to increase as well.

The MAE was very low over the first year and with advancing time slowly increased, with mean values ranging from 0.25 mm to 0.69 mm for the total GA region prediction. The MAE for the GA growth region started from 0.13 mm at 1 year to 0.72 mm at 3 years and was within the range of the MAE for the total GA region. This was in contrast to the DSC, which was numerically higher for the prediction of the total GA region compared with the prediction of the GA growth region as the DSC is very sensitive to small lesions. The metrics for all time intervals are summarized in Table 2. The values for the manual annotations and the model prediction for the total GA region and GA growth region are also summarized in Table 2.

Correlation between Ground Truth and Prediction

The correlation between progression rates derived from the manual annotations and our model predictions is shown in Figure 3. The correlation coefficient between manual and predicted progression rates calculated over the entire follow-up period of over 3 years was 0.61 with an R^2 of 0.37. Numerically, the manual ground truths and the predicted measurements of the model for the total GA region as well as the GA growth region in millimeters over the different time intervals showed similar values. In general, the mean values of the predicted GA growth regions in millimeters were numerically slightly smaller than the manual ground truth annotations over time.

Identification of Fast Progressors

The classification performance of the model to identify fast progressors for different cut-off values, i.e., the top 10%, 15%, and 20% of GA growth rates of all patients was evaluated by the area under the curve. The predictive model for the identification of fast progressors versus slow progressors produced a receiver operating characteristic curve with an area under the curve of 0.81 for the top 10%, 0.79 for the top 15%, and 0.77 for the top 20% as shown in Figure 4. The optimal operating point (Yuoden index) had a sensitivity and specificity of 0.73 and 0.91 for the top 10%, 0.73 and 0.88 for the top 15%, and 0.66 and 0.90 for the top 20%, respectively.

Discussion

Several imaging features have been found to predict faster disease progression in GA. For example, the presence of intraretinal hyperreflective foci has been shown to correlate with the conversion from intermediate AMD to late AMD and with GA progression.[20,21] On OCT, the condition of the photoreceptor layer has gained special interest as a relevant predictor of GA growth.[22,23] It has been demonstrated that photoreceptor loss and thinning precedes and exceeds GA growth and correlates with GA growth rates. In general, studies have found higher growth rates for multifocal lesions, irregularly shaped lesions, and extrafoveal lesions

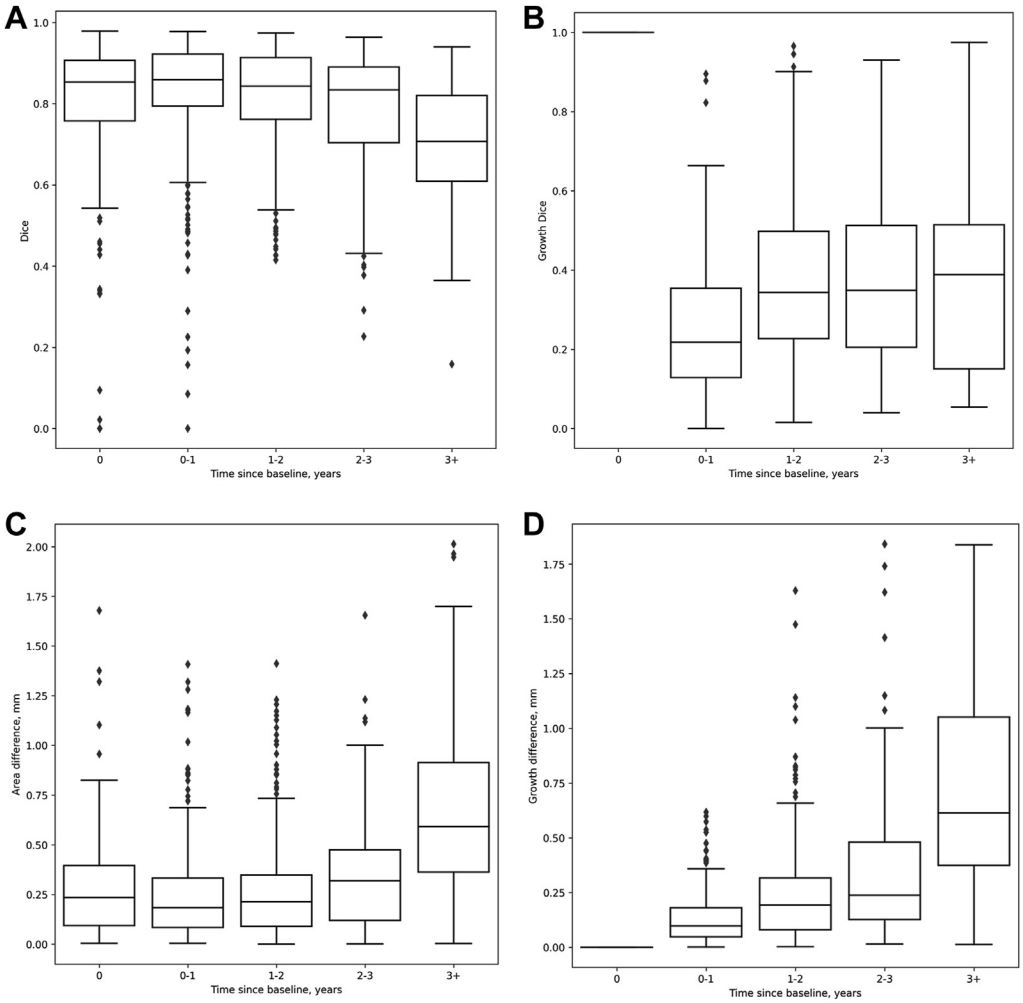

Figure 2. Boxplots of dice similarity coefficient (DSC) and mean absolute error (MAE) for total geographic atrophy (GA) region prediction and GA growth region prediction. **A,** Distribution of the DSC for the total GA region prediction. **B,** Distribution of the DSC for the GA growth region prediction. **C,** Distribution of the MAE in mm for the total GA region prediction. **D,** Distribution of the MAE in mm for the GA growth region prediction over time.

compared with unifocal, circular, and foveal lesions.[24–26] On FAF, perilesional FAF patterns labeled as banded or diffuse were suggested to be associated with faster progression than lesions with no abnormal or focal FAF patterns.[27] However, all those imaging features have been investigated at a population level and the individual disease progression of GA growth rate still remains an overwhelming challenge.

Table 2. Performance Metrics of the Algorithm Predictions for GA Growth over Time

Performance Metric	Time				
	t = 0 (baseline)	0 < t < 1	1 < t < 2	2 < t < 3	t > 3
OCT volume (n)	184	296	260	148	79
GT for total GA region (mm)	2.43 ± 1.05	2.64 ± 1.08	2.97 ± 1.08	3.25 ± 1.05	3.56 ± 1.18
Predicted total GA region (mm)	2.50 ± 0.81	2.75 ± 0.88	2.96 ± 0.92	3.11 ± 0.96	3.18 ± 1.05
DSC for total GA region	0.80 ± 0.19	0.82 ± 0.15	0.82 ± 0.13	0.77 ± 0.15	0.70 ± 0.15
MAE for total GA region (mm)	0.28 ± 0.26	0.25 ± 0.25	0.28 ± 0.27	0.35 ± 0.29	0.69 ± 0.47
GT for GA growth region (mm)	–	0.25 ± 0.22	0.52 ± 0.36	0.75 ± 0.42	1.31 ± 0.68
Predicted GA growth region (mm)	–	0.27 ± 0.13	0.42 ± 0.21	0.53 ± 0.26	0.74 ± 0.49
DSC for GA growth region	–	0.25 ± 0.16	0.38 ± 0.20	0.38 ± 0.21	0.37 ± 0.23
MAE for GA growth region (mm)	–	0.13 ± 0.11	0.25 ± 0.24	0.35 ± 0.34	0.72 ± 0.48

DSC = dice similarity coefficient; GA = geographic atrophy; GT = ground truth; MAE = mean absolute error; t = time in years.

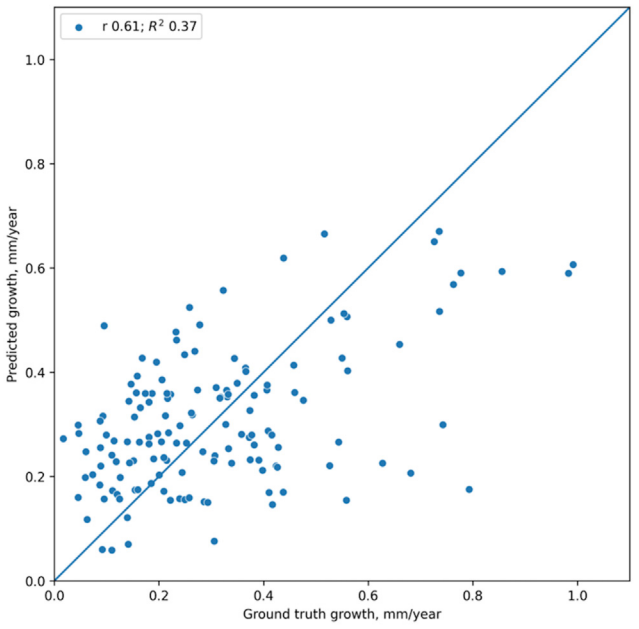

Figure 3. Scatterplot for the correlation between manual ground truth and predicted geographic atrophy growth rate in mm/year.

Our proposed algorithm is able to individually predict GA growth from a single baseline OCT volume in a time-continuous fashion using deep learning. We provided robust evidence for achieving GA growth prediction over 3 years of follow-up and obtained interpretable outputs by providing en face maps for future GA localization. This personalized atrophy growth risk map represents a clinically useful tool to understand a patient's prognosis and risk profile from the baseline visit when patients are being seen for the first time and whenever treatment decisions have to be made. The model reached a mean DSC for the prediction of the total GA growth region of 0.70 to 0.82. The DSC slightly increased for the progression prediction of up to 2 years. With increasing time of $\geq$ 3 years, the DSC slightly decreased for total GA region recognition, indicating a higher uncertainty with longer time intervals as long as $\geq$ 3 years. However, only limited follow-up data was available in year 3. We believe that the algorithm would benefit from more extensive and long-term follow-up data. When considering specific GA growth regions, the mean DSC was numerically lower, ranging from 0.25 to 0.38. However, the GA growth region represents a substantially smaller region after excluding the baseline GA region. With increasing time and increasing GA growth, the DSC for the GA growth region slightly increased as well. Prediction of biological activity in disease progression over several years is a most ambitious goal, particularly in AMD, which has been recognized as a multifactorial disease process including many endogenous as well as exogenous pathophysiological contributors. The OCT can refer to most of the relevant features located within the retinal layers; however, a standard OCT will not identify changes in choroidal perfusion such as flow voids seen only using experimental swept-source OCT devices.[28] Choroidal vascular changes in elderly individuals will substantially advance over the duration of several years. Genetic predisposition is another known factor impacting GA development and progression.[29,30] However, as SD-OCT is the major device ubiquitously available and is the core modality in the management of macular disease, particularly in AMD, it is the ideal prediction tool when equipped with artificial intelligence-based prediction capacities. Moreover, the clinical follow-up of AMD in its nonneovascular and neovascular presentation has to be tight to not miss novel changes threatening visual acuity, such as fluid. A precise prediction of GA growth activity for as long as 1 year is most useful and is easily repeated in yearly intervals, if not in continuous regular monitoring for optimal adjustment of invasive therapy or threatening foveal involvement in juxtafoveal lesions.

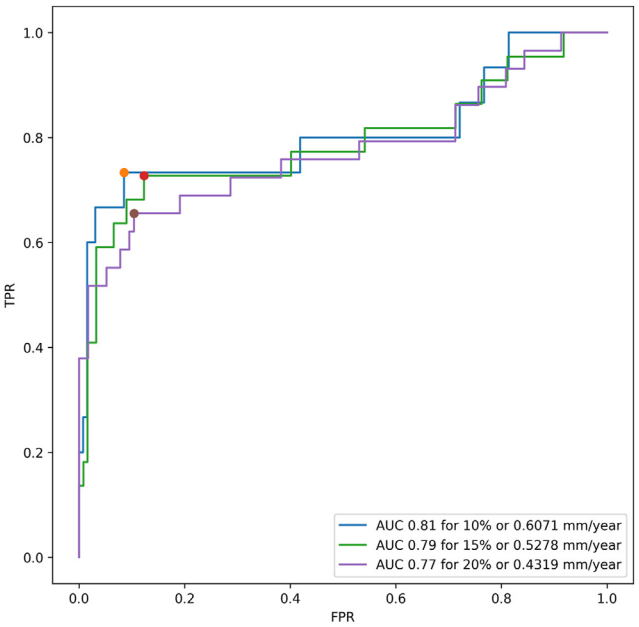

Figure 4. Area under the curve (AUC) for the identification of fast progressors for different cut-off values of the top 10%, 15%, and 20% of geographic atrophy lesion growth rate. Dots = operating points; FPR = false positive rate; TPR = true positive rate.

One known disadvantage of the DSC is its sensitivity to small areas. Therefore, we included an additional performance metric for the evaluation of the model, namely the MAE. This metric does not depend on the size of the evaluated area, as it assesses the absolute area error. The computed values for the MAE showed only small area errors for the prediction of the total GA region (0.25–0.96 mm) as well as for the GA growth region (0.13–0.72 mm), with only slowly increasing values with longer time intervals. In contrast to the DSC, the MAE indicated similar values for both the total GA region as well as the GA growth region alone. As seen in Figure 2, inaccuracies in the prediction could be caused by new satellites or because of the GA expansion within the foveal region. However, both the DSC and the MAE do not provide information on the localization of the predicted segmentation. Therefore, the inaccuracies of the localization can only be evaluated

qualitatively instead of quantitatively. In addition to the segmentation metrics, we evaluated the correlation of the predicted progression rate with the manual ground truth annotations. In this pilot study performed in a small population from clinical routine, the model reached a correlation coefficient of 0.61, indicating a moderate correlation between the predicted and the manual GA growth. Further training and validation on more extensive data are clearly needed to optimize the performance.

There have been a few previous studies which introduced different models for GA growth prediction on OCT. Previous work by our group showed that the accumulation of hyperreflective foci in the junctional zone around the atrophic lesion predicts the local progression of GA and indicates where and whether the atrophic lesion will expand. However, a global GA progression prediction was not possible.[20] Other proposed models for GA growth prediction reached a DSC of 0.81 to 0.87[31] and 0.86 to 0.92.[32] However, they were strongly limited in population size, with 29 and 25 patients, respectively. Those studies could show that taking into account more information from a patient resulted in higher DSC.[31] By taking the OCT volume from the baseline and the first follow-up visit as an input, the model reached better performance than by taking just the baseline OCT volume as an input. However, this approach requires retraining the model for every new patient.[31] Moreover, some approaches automatically extracted known risk factors of GA growth to improve the model's performance.[31] Another recent study proposed a model for personalized atrophy risk mapping with similar results.[33] The algorithm reached a DSC for the prediction of the total GA area of 0.73 to 0.80 and for the GA growth area of 0.46 to 0.72. However, this model was based on en face layer thickness and reflectivity, which is dependent on accurate layer segmentation.[33] A study by Anegondi et al[34] used a multimodal approach with FAF-only, OCT-only, and FAF and OCT together as inputs. The performance was evaluated using the squared correlation coefficient and reached an r^2 of 0.91 for the GA lesion area prediction and an r^2 of 0.36 for the GA growth rate prediction for the OCT-only approach. The prediction from a single FAF image reached an r^2 of 0.96 for GA lesion area and 0.48 for GA growth rate prediction, respectively. The FAF-only approach showed a high performance also in independent data sets. Both models achieved better performances than the reference model using baseline clinical features. This suggests that FAF and OCT images provide further information compared with anatomic features graded by human experts.[34] The proposed models were evaluated with regard to covariate adjustment to increase the power of clinical trials, rather than implementation in clinical practice. Moreover, the prediction was limited to the future overall lesion size without prediction of the future lesion localization which is, however, most relevant in the management of GA regarding foveal involvement.

In addition to the prediction of GA lesion growth and localization, we evaluated the ability of the algorithm to identify fast progressors. The algorithm was able to identify different progression profiles by correctly classifying fast progressors versus slow progressors. With the first treatment for GA being implemented in clinical practice, this represents an important clinical tool for physicians to understand disease activity in an individual patient and potential treatment benefits. With the first Food and Drug Administration-approved treatment for wide clinical use, i.e., pegcetacoplan, a complement C3 inhibitor, physicians, patients, and payers will be confronted with a huge challenge in management decisions.[35] Complement inhibition showed phase III efficacy and safety data for the treatment of GA secondary to AMD and was able to significantly reduce GA growth rate in treated patients compared with sham injections. However, we know that there is a high interindividual variability in GA growth rates, and not every patient might benefit from a clinically relevant treatment effect. The difference between sham and treatment was nevertheless moderate in an allcomer population and one has to assume that the spectrum of benefit size is very wide with a population of patients showing large benefit and others showing little benefit. Using artificial intelligence-based photoreceptor analyses, our group has already shown that the ratio of photoreceptor integrity loss versus RPE loss area is a convincing predictor for disease activity as well as the therapeutic benefit in GA.[36] Geographic atrophy grows in an unpredictable manner even for experienced ophthalmologists and under these perspectives, correctly identifying patients and lesions that are at high risk of fast progression is therefore of vital interest to plan therapeutic approaches tailored to the patient's risk profile. Moreover, newly developed treatments will be costly and needed for long-term use; therefore, knowing which patients might benefit the most from such treatments will be essential regarding socioeconomic efforts. Moreover, OCT has not been routinely introduced into monitoring GA disease, and treatment standards have yet to be established. To provide the base for an efficient learning curve in GA management, OCT-based tools providing reliable parameters will help to introduce urgently needed guidance, paving the way into the era of individualized risk assessment and objective decision-making processes in GA patients, which is highly needed after approval of the first paradigm-shifting therapy.

Limitations of our study include a possible selection bias due to the exclusion of patients with other retinal diseases and images with bad quality. Also, the model was trained and evaluated on Spectralis scans only. More studies are needed to investigate the performance of the algorithm on OCT images of other devices and mixed cases. Furthermore, the automated registration of FAF-based annotations to OCT might lead to some discrepancies. On the other hand, automated registration of different retinal imaging modalities such as OCT and FAF allows the use of more imaging data without the need for manual annotations of every modality with laborious efforts. There could be a correlation in growth rates between fellow eyes as the study population derives from clinical routine patients. Moreover, the proposed algorithm is not able to predict functional deficits. However, knowing which patients are at risk of faster progression and therefore might benefit most from treatment is an important clinical decision support tool for physicians. Assessing functional deficits and risk of visual loss is very difficult in GA patients as the routinely collected best-

corrected visual acuity in clinics does not reflect the disease activity. To be implemented in clinical practice, the algorithm would need further external validation and extension on more clinical data. However, this proof-of-concept has shown that fully automated prediction of GA lesion growth only from the baseline OCT is feasible. Another strength of our analysis is the use of consecutively collected data from routine clinical care for the evaluation and testing of the algorithm.

In summary, we could show that the algorithm is capable of fully automated GA lesion growth prediction from a single baseline OCT volume in a time-continuous fashion. The algorithm provides interpretable outputs in the format of en face maps showing future GA growth and localization as a clinically relevant tool. Moreover, the algorithm was able to correctly identify fast progressors and hence patients who have a high risk of rapid disease progression, which supports the assessment of objective metrics for targeted interventions. The results of this pilot study are a promising step toward clinical decision support tools for therapeutic dosing and guidance of patient management on a large scale, now that the first treatment for GA has finally become available.

Footnotes and Disclosures

Originally received: July 24, 2023.
Final revision: November 8, 2023.
Accepted: January 9, 2024.
Available online: January 17, 2024.Manuscript no. XOPS-D-23-00185R1.

OPTIMA - Laboratory for Ophthalmic Image Analysis, Department of Ophthalmology and Optometry, Medical University of Vienna, Vienna, Austria.

Presented, in parts, at the Annual Meeting of the Association of Research in Vision and Ophthalmology, May 1-7, 2021, Virtual.

Disclosure(s):

All authors have completed and submitted the ICMJE disclosures form.

The author(s) have made the following disclosure(s): G.S.R.: Contract research – RetInSight.

H.B.: Contract research – Apellis, Heidelberg Engineering; Payment or honoraria for lectures – Bayer, Roche, Apellis.

U.S.-E.: Grants or contracts – Abbvie, Boehringer, Genentech, Heidelberg Engineering, Janssen, Kodiak, Novartis, Roche, RetInSight, Apellis Pharmaceuticals; Scientific consultant – Apellis, Roche; Payment or honoraria for lectures – Roche, Apellis; Travel support - Abbvie, Apellis; Participation on a Data Safety Monitoring Board or Advisory Board – Abbvie, Apellis.

The other authors have no proprietary or commercial interest in any materials discussed in this article.

HUMAN SUBJECTS: Human subjects were included in this study. The presented study was approved by the ethics ommittee of the Medical University of Vienna (EK Nr: 1246/2016). All research was performed in compliance with the tenets of the Declaration of Helsinki and Good Clinical Practice. Written informed consent was given by all patients for future medical research and analyses.

No animal subjects were used in this study.

Author Contributions:

Conception and design: Mai, Lachinov, Reiter, Riedl, Bogunovic, Schmidt-Erfurth

Data collection: Mai, Lachinov, Reiter, Grechenig, Bogunovic, Schmidt-Erfurth

Analysis and interpretation: Mai, Lachinov, Reiter, Bogunovic, Schmidt-Erfurth

Obtained funding: N/A

Overall responsibility: Schmidt-Erfurth

Abbreviations and Acronyms:
AMD = age-related macular degeneration; **DSC** = dice similarity coefficient; **FAF** = fundus autofluorescence; **GA** = geographic atrophy; **MAE** = mean absolute error; **OCT** = optical coherence tomography; **ODE** = ordinary differential equation; **RPE** = retinal pigment epithelium; **SD-OCT** = spectral-domain OCT.

Keywords:
Artificial intelligence, Geographic atrophy, Geographic atrophy progression, Optical coherence tomography.

Correspondence:
Ursula Schmidt-Erfurth, MD, Department of Ophthalmology, Medical University of Vienna Spitalgasse 23, 1090 Vienna, Austria. E-mail: ursula.schmidt-erfurth@meduniwien.ac.at.

References

1. Ferris III FL, Wilkinson CP, Bird A, et al. Clinical classification of age-related macular degeneration. *Ophthalmology*. 2013;120:844–851. https://doi.org/10.1016/j.ophtha.2012.10.036.
2. Miller JW, Bagheri S, Vavvas DG. Advances in age-related macular degeneration understanding and therapy. *US Ophthal Rev*. 2017;10:119–130. https://doi.org/10.17925/USOR.2017.10.02.119.
3. Friedman DS, O'Colmain BJ, Muñoz B, et al. Prevalence of age-related macular degeneration in the United States. *Arch Ophthalmol*. 2004;122:564–572. https://doi.org/10.1001/archopht.122.4.564.
4. Wong WL, Su X, Li X, et al. Global prevalence of age-related macular degeneration and disease burden projection for 2020 and 2040: a systematic review and meta-analysis. *Lancet Glob Health*. 2014;2:e106–e116. https://doi.org/10.1016/S2214-109X(13)70145-1.
5. Schmitz-Valckenberg S, Sahel JA, Danis R, et al. Natural history of geographic atrophy progression secondary to age-related macular degeneration (geographic atrophy progression study). *Ophthalmology*. 2016;123:361–368. https://doi.org/10.1016/j.ophtha.2015.09.036.
6. Khanani AM, Patel SS, Staurenghi G, et al. Efficacy and safety of avacincaptad pegol in patients with geographic atrophy (GATHER2): 12-month results from a randomised, double-masked, phase 3 trial. *Lancet*. 2023;402:1449–1458. https://doi.org/10.1016/S0140-6736(23)01583-0.
7. Heier JS, Lad EM, Holz FG, et al. Pegcetacoplan for the treatment of geographic atrophy secondary to age-related macular degeneration (OAKS and DERBY): two multicentre,

randomised, double-masked, sham-controlled, phase 3 trials. *Lancet*. 2023;402:1434−1448. https://doi.org/10.1016/S0140-6736(23)01520-9.
8. Göbel AP, Fleckenstein M, Schmitz-Valckenberg S, Brinkmann CK, Holz FG. Imaging geographic atrophy in age-related macular degeneration. *Ophthalmologica*. 2011;226:182−190. https://doi.org/10.1159/000330420.
9. Cleland SC, Konda SM, Danis RP, et al. Quantification of geographic atrophy using spectral domain OCT in age-related macular degeneration. *Ophthalmol Retina*. 2021;5:41−48. https://doi.org/10.1016/j.oret.2020.07.006.
10. Guymer RH, Rosenfeld PJ, Curcio CA, et al. Incomplete retinal pigment epithelial and outer retinal atrophy in age-related macular degeneration: classification of atrophy meeting Report 4 Report 4. *Ophthalmology*. 2020;127:394−409. https://doi.org/10.1016/j.ophtha.2019.09.035.
11. Schaal KB, Rosenfeld PJ, Gregori G, Yehoshua Z, Feuer WJ. Anatomic clinical trial endpoints for nonexudative age-related macular degeneration. *Ophthalmology*. 2016;123:1060−1079. https://doi.org/10.1016/j.ophtha.2016.01.034.
12. Wang J, Ying GS. Growth rate of geographic atrophy secondary to age-related macular degeneration: a meta-analysis of natural history studies and implications for designing future trials. *Ophthal Res*. 2021;64:205−215. https://doi.org/10.1159/000510507.
13. Fleckenstein M, Mitchell P, Freund KB, et al. The progression of geographic atrophy secondary to age-related macular degeneration. *Ophthalmology*. 2018;125:369−390. https://doi.org/10.1016/j.ophtha.2017.08.038.
14. Bui PTA, Reiter GS, Fabianska M, et al. Fundus autofluorescence and optical coherence tomography biomarkers associated with the progression of geographic atrophy secondary to age-related macular degeneration. *Eye (Lond)*. 2022;36:2013−2019. https://doi.org/10.1038/s41433-021-01747-z.
15. Arikan M, Sadeghipour A, Gerendas B, Told R, Schmidt-Erfurt U. In: *Deep learning based multi-modal registration for retinal imaging. In: Interpretability of Machine Intelligence in Medical Image Computing and Multimodal Learning for Clinical Decision Support. Second International Workshop, iMIMIC 2019, and 9th International Workshop, ML-CDS 2019, Held in Conjunction with MICCAI 2019*. Shenzhen, China: Springer International Publishing; 2019:75−82.
16. Lachinov D, Chakravarty A, Grechenig C, Schmidt-Erfurth U, Bogunovic H. Learning spatio-temporal model of disease progression with NeuralODEs from longitudinal volumetric data. *IEEE Trans Med Imaging*. 2023. https://doi.org/10.1109/TMI.2023.3330576.
17. Lachinov D, Seeböck P, Mai J, Goldbach F, Schmidt-Erfurth U, Bogunovic H. Projective skip-connections for segmentation along a subset of dimensions in retinal OCT. In: de Bruijne M, et al., eds. Med Image Comput Assist Interv MICCAI. *MICCAI 2021*. Cham: Springer; 2021:431−441. Lecture Notes in Computer Science; 12901.
18. Chen RT, Rubanova Y, Bettencourt J, Duvenaud DK. Neural ordinary differential equations. *Adv Neural Inf Process Syst*. 2018;31.
19. Feuer WJ, Yehoshua Z, Gregori G, et al. Square root transformation of geographic atrophy area measurements to eliminate dependence of growth rates on baseline lesion measurements: a reanalysis of Age-Related Eye Disease Study Report No. 26. *JAMA Ophthalmol*. 2013;131:110−111. https://doi.org/10.1001/jamaophthalmol.2013.572.
20. Schmidt-Erfurth U, Bogunovic H, Grechenig C, et al. Role of deep learning-quantified hyperreflective foci for the prediction of geographic atrophy progression. *Am J Ophthalmol*. 2020;216:257−270. https://doi.org/10.1016/j.ajo.2020.03.042.
21. Waldstein SM, Vogl WD, Bogunovic H, Sadeghipour A, Riedl S, Schmidt-Erfurth U. Characterization of drusen and hyperreflective foci as biomarkers for disease progression in age-related macular degeneration using artificial intelligence in optical coherence tomography. *JAMA Ophthalmol*. 2020;138:740−747. https://doi.org/10.1001/jamaophthalmol.2020.1376.
22. Reiter GS, Told R, Schranz M, et al. Subretinal drusenoid deposits and photoreceptor loss detecting global and local progression of geographic atrophy by SD-OCT imaging. *Invest Ophthalmol Vis Sci*. 2020;61:11. https://doi.org/10.1167/iovs.61.6.11.
23. Pfau M, von der Emde L, de Sisternes L, et al. Progression of photoreceptor degeneration in geographic atrophy secondary to age-related macular degeneration. *JAMA Ophthalmol*. 2020;138:1026−1034. https://doi.org/10.1001/jamaophthalmol.2020.2914.
24. Shen LL, Sun M, Grossetta Nardini HK, Del Priore LV. Progression of unifocal versus multifocal geographic atrophy in age-related macular degeneration: a systematic review and meta-analysis. *Ophthalmol Retina*. 2020;4:899−910. https://doi.org/10.1016/j.oret.2020.03.020.
25. Domalpally A, Danis RP, White J, et al. Circularity index as a risk factor for progression of geographic atrophy. *Ophthalmology*. 2013;120:2666−2671. https://doi.org/10.1016/j.ophtha.2013.07.047.
26. Shen LL, Sun M, Khetpal S, Grossetta Nardini HK, Del Priore LV. Topographic variation of the growth rate of geographic atrophy in nonexudative age-related macular degeneration: A systematic review and meta-analysis. *Invest Ophthalmol Vis Sci*. 2020;61:2. https://doi.org/10.1167/iovs.61.1.2.
27. Holz FG, Bindewald-Wittich A, Fleckenstein M, et al. Progression of geographic atrophy and impact of fundus autofluorescence patterns in age-related macular degeneration. *Am J Ophthalmol*. 2007;143:463−472. https://doi.org/10.1016/j.ajo.2006.11.041.
28. Braun PX, Mehta N, Gendelman I, et al. Global analysis of macular choriocapillaris perfusion in dry age-related macular degeneration using swept-source optical coherence tomography angiography. *Invest Ophthalmol Vis Sci*. 2019;60:4985−4990. https://doi.org/10.1167/iovs.19-27861.
29. Fritsche LG, Igl W, Bailey JN, et al. A large genome-wide association study of age-related macular degeneration highlights contributions of rare and common variants. *Nat Genet*. 2016;48:134−143. https://doi.org/10.1038/ng.3448.
30. Agrón E, Domalpally A, Cukras CA, et al. Reticular pseudodrusen status, ARMS2/HTRA1 genotype, and geographic atrophy enlargement: Age-Related Eye Disease Study 2 Report 32. *Ophthalmology*. 2023;130:488−500. https://doi.org/10.1016/j.ophtha.2022.11.026.
31. Niu S, de Sisternes L, Chen Q, Rubin DL, Leng T. Fully automated prediction of geographic atrophy growth using quantitative spectral-domain optical coherence tomography biomarkers. *Ophthalmology*. 2016;123:1737−1750. https://doi.org/10.1016/j.ophtha.2016.04.042.
32. Zhang Y, Zhang X, Ji Z, et al. An integrated time adaptive geographic atrophy prediction model for SD-OCT images. *Med Image Anal*. 2021;68:101893. https://doi.org/10.1016/j.media.2020.101893.
33. Gigon A, Mosinska A, Montesel A, et al. Personalized atrophy risk mapping in age-related macular degeneration. *Transl Vis Sci Technol*. 2021;10:18. https://doi.org/10.1167/tvst.10.13.18.

34. Anegondi N, Gao SS, Steffen V, et al. Deep learning to predict geographic atrophy area and growth rate from multimodal imaging. *Ophthalmol Retina*. 2023;7:243–252. https://doi.org/10.1016/j.oret.2022.08.018.
35. Liao DS, Grossi FV, El Mehdi D, et al. Complement C3 inhibitor pegcetacoplan for geographic atrophy secondary to age-related macular degeneration: a randomized Phase 2 trial. *Ophthalmology*. 2020;127:186–195. https://doi.org/10.1016/j.ophtha.2019.07.011.
36. Riedl S, Vogl WD, Mai J, et al. The effect of pegcetacoplan treatment on photoreceptor maintenance in geographic atrophy monitored by artificial intelligence-based OCT analysis. *Ophthalmol Retina*. 2022;6:1009–1018. https://doi.org/10.1016/j.oret.2022.05.030.